Available online at www.sciencedirect.com
ScienceDirect
Vision Research 47 (2007) 1178–1190
Vision Research
www.elsevier.com/locate/visres

Emmetropization and schematic eye models in developing pigmented guinea pigs

Marcus H.C. Howlett, Sally A. McFadden *

School of Psychology, Faculty of Science and Information Technology, The University of Newcastle, NSW 2308, Australia

Received 20 September 2006; received in revised form 9 December 2006

Abstract

A model of the axial change in ocular parameters of the guinea pig eye from 2 to 825 days of age was developed and a corresponding paraxial schematic eye model applicable from 2 to 100 days of age was constructed. Axial distances increased logarithmically over time except for the lens in which growth was more complex. Over the first 30 days, ocular elongation was approximately linear: ocular length increased by 37 μm/day, the majority due lens expansion. The choroid and sclera thickened with age, while the retina thinned in proportion to the increased ocular size, and the model suggests that there is no small eye artefact for white light retinoscopy. Refractive error just after birth was +4.8 D but halved within the first week. Emmetropization occurred within the first month of life similar to that in other species when aligned at the point of sexual maturity and scaled by the time taken to reach adulthood. The power of the eye was 227 D at 2 days of age and reduced by 19.7 D by 100 days due to a 22% decrease in the power of the cornea. The posterior nodal distance (PND) was 4.7 mm at 30 days of age, with a maximum rate of change of 13 μm/day during the first week. The ratio of PND to axial length declined until at least 100 days of age, well after emmetropia was reached. This suggests that the maintenance of emmetropia is not sustained through proportional axial growth, but involves some active mechanism beyond simple scaling. The model predicts that 1 D of myopia requires an elongation of between 23 and 32 μm, depending upon age, suggesting that a resolution of at least 50 μm is required in methods used to determine the significance of ocular length changes in guinea pig models of refractive development. Retinal magnification averaged 80 μm/degree, and the maximum potential brightness of the retinal image was high, which together with a ratio of lens power to corneal power of 1.7–2.0 suggests that the guinea pig eye is adapted for noctural conditions.

Keywords: Schematic eye; Refractive error; Axial length; Emmetropization; Growth; Guinea pig; Cornea; Lens; Retina; Power

1. Introduction

Emmetropia is characterised by a match between the power of the optics and the axial length of the eye so that in the absence of accommodation, distant images are focussed at the photoreceptor layer. Emmetropization is the process of achieving emmetropia and involves a reduction in the refractive error that is present at birth. The human newborn refractive state varies between individuals (Cook & Glasscock, 1951; Gwiazda, Thorn, Bauer, & Held, 1993; Sorsby & Sheridan, 1960) and some species are born myopic (kestrel: Andison, Sivak, & Bird, 1992; ostrich: Ofri et al., 2001) but in most species, the newborn eye is hyperopic and over time becomes emmetropic (chick: Wallman, Adams, & Trachtman, 1981; mouse: Schmucker & Schaeffel, 2004; tree shrew: Norton & McBrien, 1992; marmoset: Graham & Judge, 1999; Troilo & Judge, 1993; rhesus monkey: Bradley, Fernandes, Lynn, Tigges, & Boothe, 1999; human: Ehrlich, Atkinson, Braddick, Bobier, & Durden, 1995; Gwiazda et al., 1993; Mayer, Hansen, Moore, Kim, & Fulton, 2001; Saunders, Woodhouse, & Westall, 1995; Sorsby, Benjamin, & Sheridan, 1961; Wood, Hodi, & Morgan, 1995). In many species studied, ocular components of the eye, notably the lens, continue to change and eye growth occurs beyond the time that initial emmetropia is obtained. Thus the eye also needs to

* Corresponding author. Fax: +61 249 216980.
E-mail address: sally.mcfadden@newcastle.edu.au (S.A. McFadden).

0042-6989/$ - see front matter
doi:10.1016/j.visres.2006.12.019

maintain emmetropia. It is undisputed that emmetropization is in part actively achieved through visual feedback (for a recent review see Wallman & Winawer, 2004). Less is known about the processes underlying the maintenance of emmetropia.

Since the process of emmetropization and the maintenance of emmetropia is affected by the relative growth of the various ocular components, it is important to carefully characterise ocular growth in a variety of species. The guinea pig eye provides a useful model to study the regulation of ocular growth which is partially controlled by visual input and the associated retinal activity (Howlett & McFadden, 2006; Lu et al., 2006; McFadden, Howlett, & Mertz, 2004). Key aspects of retinal development in the guinea pig eye are similar to humans (Loeliger & Rees, 2005; Spira, 1975). The guinea pig eye has also been used as a model to study a variety of factors which are effected by ocular development, including the cornea (Castro, Lutz, & Edelman, 2004; Foster, Zelt, Mai-Phan, & Kenyon, 1982), crystalline lens (Simpanya, Ansari, Suh, Leverenz, & Giblin, 2005) and retinal development (Loeliger & Rees, 2005). The interpretation of many of these studies would be aided by the development of schematic eye applicable to any age. A first-order paraxial schematic eye can be used to understand refractive errors including astigmatism, chromatic aberration, the size of the image on the retina and the blur associated with defocus (Westheimer, 2006). A description of some aspects of the normal ocular development of the guinea pig eye is available up to 11 weeks of age (Zhou et al., 2006). In this paper, we sought to accurately describe the ocular development of axial parameters in guinea pigs, and measured animals aged from 2 to 825 days of age. Additionally, we determined key aspects of optical development which we used to construct a paraxial schematic eye model applicable from 2 to 100 days of age.

2. Methods

2.1. Animals

Pigmented guinea pigs (*Cavia porcellus*, $n = 183$) aged from birth to 825 days were maternally reared until they were weaned at three weeks of age. They were then housed in groups of 2–3, in opaque plastic boxes ($65 \times 45 \times 20$ cm) with wire mesh lids. Each box had a small hiding area under a stainless steel shelf ($32 \times 16 \times 14$ cm) and the floor was covered with wood shavings. Water (supplemented with Vitamin C), guinea pig food pellets, and hay were available *ad libitum*, and mixed vegetable pieces were occasionally provided. Ceiling lights (36 W daylight fluorescent tubes) were switched on a 12 h light/12 h dark cycle. The room temperature was 22 °C. All procedures were approved by The University of Newcastle in accordance with NSW Animal Research Act and were in accordance with NIH Guidelines.

2.2. Refractive error

Refractive error was measured by streak retinoscopy in hand-held, awake animals in which cycloplegia had been induced 15–20 min prior to measurement with 1% cyclopentolate. We found it was important to bathe the cornea with cyclopentolate for approximately 10 min by holding the animal so that the eye was horizontal. We have found this to be an effective method to rapidly induce cycloplegia since in a separate longitudinal study, we found that guinea pigs refracted in the same manner and time frame with and without cycloplegia were consistently more hyperopic with cycloplegia (average difference of $+3.0 \pm 0.9$ D over the first 30 days, $n = 7$, $p < 0.001$). Furthermore, no pupil response was observed once cycloplegia was induced, and no change in the refractive state was observed during its measurement or when measured 30 min later. Refractive errors are reported as the mean of the horizontal and vertical meridians (see Fig. 1a in Howlett & McFadden, 2006). Particular care was taken to assess only the direction of movement of the retinoscopic reflex in the centre of the pupil on the optical axis (Hughes, 1977a; Mutti, Zadnik, Johnson, Howland, & Murphy, 1992).

2.3. Ultrasound measurement of axial dimensions

Axial dimensions of the eye were measured using high frequency ultrasound (20 MHz) in anaesthetised guinea pigs (1–2% Halothane in oxygen) as previously described (Howlett & McFadden, 2006; McFadden et al., 2004). The echo latencies from the different ocular tissues were transformed to distances between the surfaces based on a sound velocity of 1.534 mm/μs for all ocular tissue except for the lens which was calibrated at 1.774 mm/μs (Howlett & McFadden, 2006; McFadden et al., 2004). Peaks were selected for the front of the cornea, the front of the crystalline lens, the back of the crystalline lens, the vitreal–retinal, retinal–choridal and choridal–scleral interfaces, and the back of the sclera as previously described (see Fig. 1 in Howlett & McFadden, 2006; McFadden et al., 2004). The axial distance from the anterior corneal surface to the back of the retina was defined as the "axial length" and to the back of the sclera as the "ocular length". The thickness of the cornea was measured in 24 eyes from animals of either 3, 11 or 21 days of age using traces in which the corneal peaks were particularly clear. There was no significant difference between these three ages ($F = 1.12$, $p = .34$), so the average value (253.3 ± 2.5 μm) was used to approximate corneal thickness in all ages. The "anterior chamber depth" was the distance from the anterior corneal surface to the anterior lens surface minus this average value of the thickness of the cornea. The "posterior chamber depth" was the distance from the back of the lens to the vitreal–retinal boundary.

2.4. Infrared videokeratometry

The radius of the anterior cornea was measured in awake guinea pigs with a custom-made infrared keratometer as previously described (Howlett & McFadden, 2006). Images covered approximately 40% of the cornea and only those in which the reflection of the LED rings were centred on the pupil were digitised. Three such centred images were analysed for each eye measured. The corneal radius was determined using custom-made software and linear extrapolation based on the LED image reflected from two calibration ball bearings of known radii (3 and 4 mm). The power of the cornea was derived from the average of the four radii for each ring using the formula: $F = (n - 1)/r$, where F = anterior corneal surface power in diopters (D), n = corneal refractive index (1.336), and r = corneal radius (m). The inner 40% of the guinea pig's anterior corneal surface was approximately spherical, thus the data shown are the average power of the three rings. The maximum diameter of the entrance pupil was also determined from the images. The measurements were taken in a dark room with only infrared illumination to which the pupil reflex is insensitive and are referred to as the dark entrance pupil diameter.

2.5. Frozen sections

The radius of the anterior and posterior surfaces of the cornea and crystalline lens were determined in frozen hemisections from 16 guinea pig eyes. Animals were first anaesthetised with 2–4% halothane in oxygen, then rapidly euthanized by cardiac puncture with an overdose of pentobarbitone (lethobarb®), and the eyes were enucleated. Each eye was embedded in tissue freezing medium (Triangle Biomedical Sciences) and

rapidly frozen at −30 °C on a freezing microtome. Eyes were horizontally sectioned in 30 μm steps and magnified video images (55 pixel/mm) collected under halogen illumination. Images were digitized and measurements were taken from the mid-horizontal section for each eye defined as that with the greatest lens thickness. Surface curvatures were analysed using best spherical fits centred on the optic axis.

2.6. Refractive indices

The refractive indices of the vitreous humor and crystalline lens were measured using a calibrated Abbe refractometer in 26 fresh extracts from guinea pigs aged from 1 to 30 days. The average of 5–8 readings were calculated for each sample. The lens tissue was flattened and squashed. In three 30 day old guinea pigs, separate measurements were made of the lens core (separated by squeezing, Hughes, 1979) and the remaining lens shell. This data is included for completeness, but it should be noted that the schematic eyes were constructed using an equivalent homogeneous refractive index of the lens, and a shell based model of the lens was not attempted here.

The remaining refractive indices were taken from the literature as follows: the refractive index of the aqueous was taken to be the same as the vitreous as in previous schematic eyes (rabbit: Hughes, 1972; chick: Schaeffel, Glasser, & Howland, 1988); the refractive index of the cornea used was 1.376, the same as for the human (from Gullstrand's schematic eye) and used in the rabbit schematic eye (Hughes, 1972). The refractive index of the retina was made equal to that of the rat (1.351: Hughes, 1979).

2.7. Construction of the schematic models

Paraxial model eyes were constructed using a ray tracing program (OSLO Edu 6.3.1) and optical parameters were also determined using our own program based on standard lens formulae as described in Hughes (1972) and Helmholtz (1925). Close correspondence was found between the two methods. The model parameters for each age were derived from the fits to the data from 2 to 825 days. Ocular distances were based on ultrasound, anterior corneal curvature from infrared videokeratometry, posterior corneal curvature from adjustment to the anterior curvature based on the relative curvature proportions in frozen tissue, and the radius of the anterior and posterior lens were calculated directly from the images of the frozen mid-horizontal sections. Conventions numbered the surfaces from $A1$ to $A8$ beginning with the anterior vertex of the cornea; measurements to the right of $A1$ are positive; convex surfaces have positive radii (r); and the 1st and 2nd points are given capital letters without and with an apostrophe, respectively. Much of this nomenclature is shown in Fig. 7b.

Each schematic eye was constructed by adjusting the refractive index of the crystalline lens to match a predetermined refractive error. The model only used an equivalent homonogeneous refractive index for the crystalline lens (Vakkur & Bishop, 1963). The refractive error for each schematic eye was derived from fits to an adjusted refractive error measure based on the assumption that the guinea pig eye emmetropized to zero. Thus the models were corrected for any offset of the retinoscopic reflex from the photoreceptor plane. Each schematic eye was corrected with a lens of equivalent power to the refractive error, placed on the anterior cornea. The refractive index of a hypothetical homonogeneous crystalline lens was adjusted so that the focal plane was at the retinal/choroidal boundary as determined from the ultrasound distances. The hypothetical small eye artefact (Glickstein & Millodot, 1970) was calculated as the difference in power between the two models in which the focal plane was located at either the vitreal/retinal or retinal/choroidal boundary. The actual artefact was the value that the eye emmetropized to, estimated as being the average over the period where the refractive error was stable (30–825 days of age) defined as the period where the fitted function did not deviate more than 0.1 D.

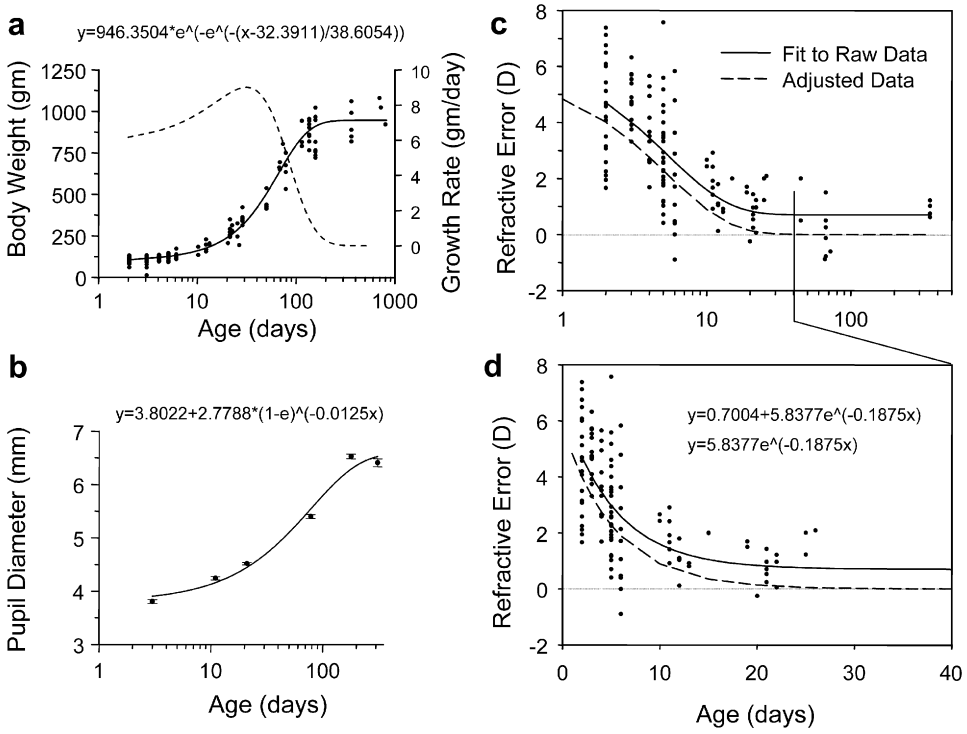

Fig. 1. Developmental changes in normal pigmented guinea pigs. (a) Body weight: filled circles and solid line (axis on left and fit equation above). Rate of change in body weight peaks at 32 days of age: dashed line (axis on right, fit equation not shown). (b) Dark pupil diameter was measured under infrared illumination to which the pupil does not respond. Standard error bars are shown. Fit (solid line) equation above. (c) Average horizontal and vertical refractive error over the entire measurement period and (d) expanded on a linear scale to show the emmetropization period in individual animals (filled circles). The two equations are the fit to the original data (solid line, first equation), and the data adjusted to true emmetropization (see text) (dashed line, second equation). The fits are the same in (c) and (d).

2.8. Data presentation and analysis

Each guinea pig was measured by ultrasound once at a selected age and the data presented is the average of the values found for the left and right eye. A cross-sectional design was used as some eyes were dissected for curvature measurements and it is feasible that repeated anaesthesia may influence ocular parameters. All fit equations were generated using regression analysis (using Sigma Plot V9). Fits were linear, $\log_{10}$ or exponential functions based on satisfaction of convergence and the principle of using the simplest possible equation which gave r^2 values >0.99. This strict criterion was necessary to ensure that the models could accurately predict a parameter at any age. Statistical tests used ANOVA and *t*-tests as indicated (using SPSS V10 for Windows and SigmaStat). Error bars on graphs are the standard error of the mean (SEM).

3. Results

3.1. Development of body mass, pupil diameter and refractive error

Body weight increased approximately linearly until 32 days of age when maximum growth rates were reached (9 gm/day), and the rate of growth declined thereafter (Fig. 1a). Maximum body weight reached a plateau at approximately 300 days of age, with daily growth slowing to less than 0.02 gm/day after 300 days. Maximum entrance pupil diameter increased rapidly until 200 days of age reach-

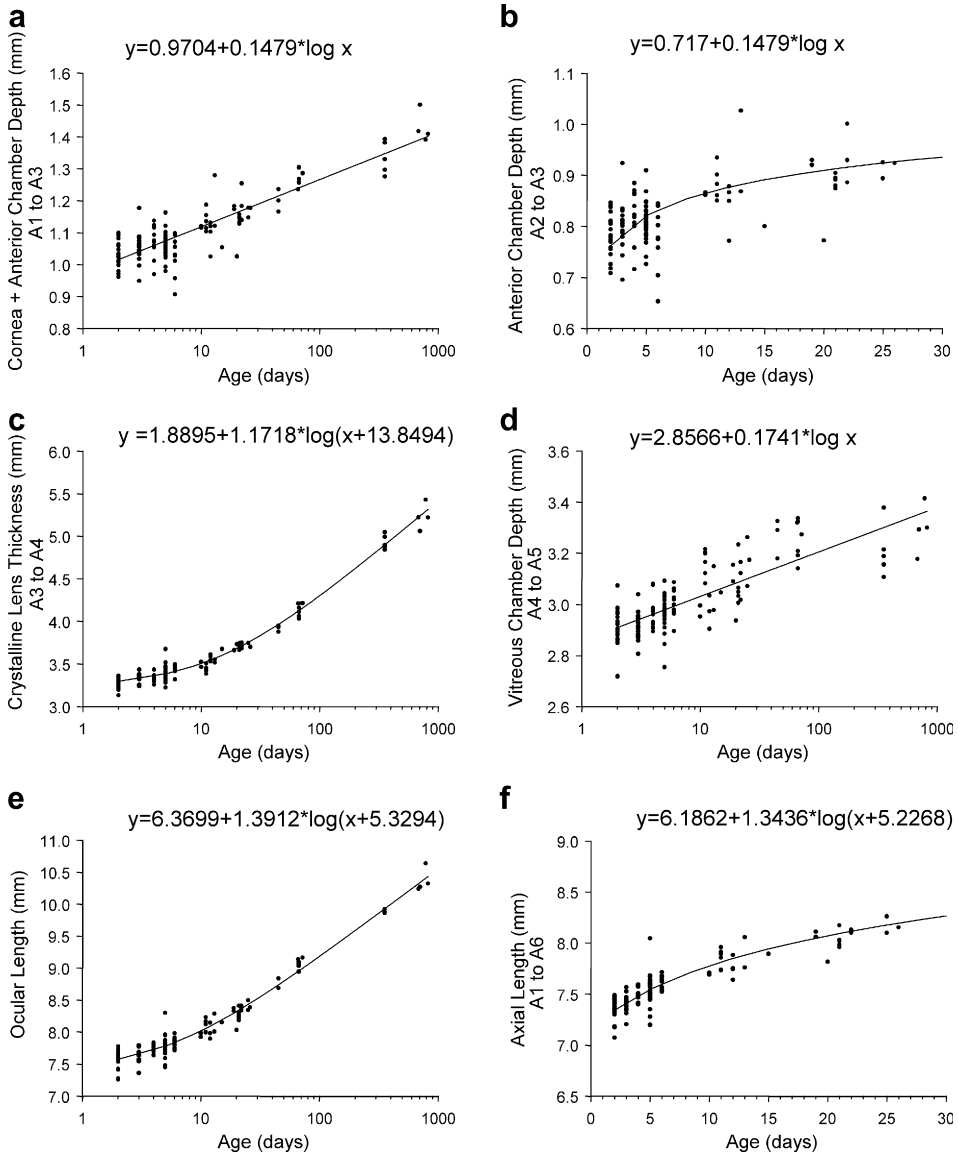

Fig. 2. Development of axial dimensions from ultrasound in anaethetised guinea pigs. (a) Distance from the anterior surface of the cornea to the anterior surface of the lens. (b) Change in the depth of the anterior chamber during the first 30 days. (c) The crystalline lens required a more complex log fit to adequately describe both young and old animals shown here on a log scale. (d) The increase in the vitreous chamber could be fitted by a simple log function. (e) Ocular length, the axial distance from the anterior cornea to the back of the sclera, required a complex log fit because the largest component is the lens. (f) Axial length over the emmetropization period. The equation for each fit (solid lines) are shown above each graph, $r^2 \geqslant 0.99$ for all fits and based on data to 850 days of age in all cases.

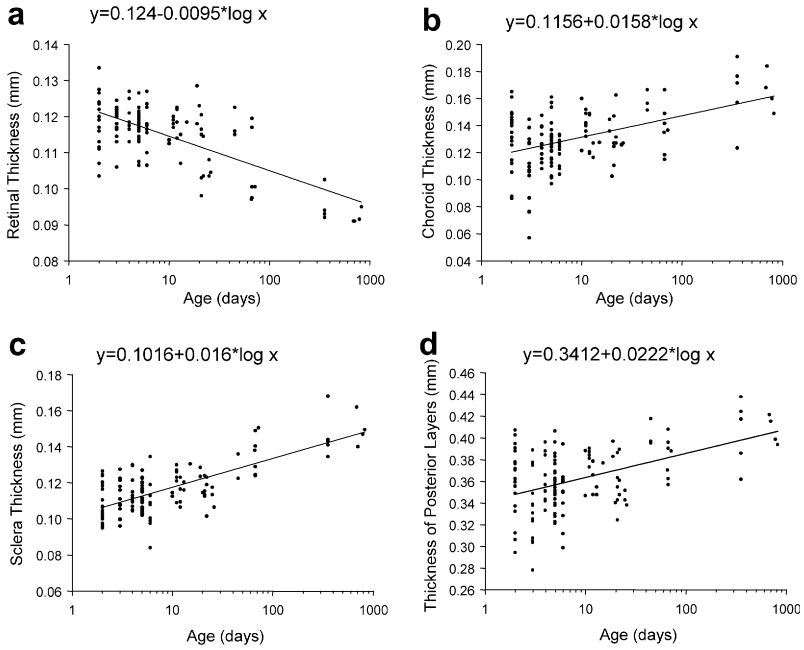

Fig. 3. Changes with age in the thickness of the (a) retina, (b) choroid, (c) sclera and (d) the total of these posterior layers measured in live guinea pigs using high-frequency ultrasound. The equation for the fit (solid lines) to the raw data (filled circles) are shown at the top of each graph.

ing a maximum diameter in adults of 6.5 mm (Fig. 1b). The rate of change in the dark entrance pupil diameter was maximal just after birth and declined with age.

Guinea pigs were on average 4.4 ± 0.4 D hyperopic 2 days after birth and rapidly developed towards emmetropia (Fig. 1c). Fits to the data suggested that a constant refractive state of +0.7 D was reached at 30 days of age, approximately the same time at which the maximum rate in body weight change occurred. If this slight hyperopia was an artefact of the refraction method and guinea pigs achieve emmetropia, then the true refractive error is shown by the dashed line in Fig. 1c, which predicts that newborn animals are 4.8 D hyperopic. The rate of emmetropization slowed with age. The initial hyperopia reduced by 55%, 65% and 83% by 6, 11 and 21 days of age, respectively (Fig. 1d). Over the first 30 days, the rate of change in refractive error was approximately −0.17 D/day. The refractive error in the primary (horizontal) meridan was 0.4 ± 0.05 D less hyperopic than the vertical ($p < .001$), indicating a tendency towards 'against the rule' astigatism.

3.2. Growth in the ocular parameters

The long term growth in ocular and axial length and the changes in the axial depth of the anterior and posterior chambers and the crystalline lens are shown in Fig. 2. The long term increases in the anterior and posterior chamber depths were best described by simple log functions, but the crystalline lens appeared to have multiple stages of growth which, together with the axial and ocular lengths, were best described by the more complex log functions shown. However, over the first 30 days, corresponding to the emmetropization period, the rate of growth was approximately linear: ocular length increased by 37 μm/day; the lens expanded in thickness at twice the rate

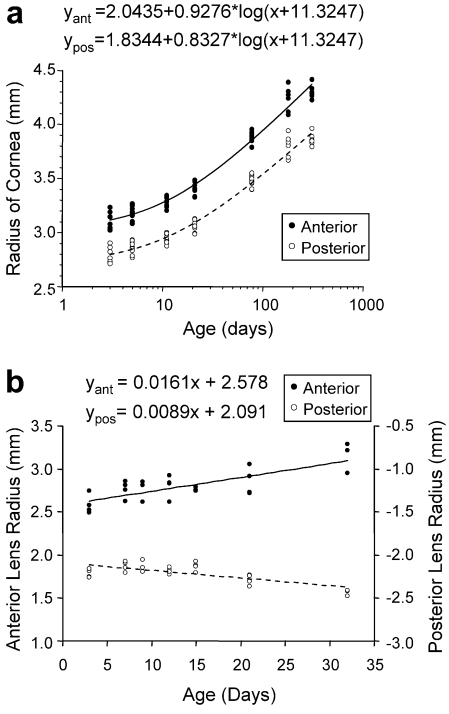

Fig. 4. Changes with age in the radii of curvature of the cornea and lens. (a) Corneal radius: The anterior (ant) curvature (solid line, 1st equation) was measured with infrared keratometry in awake guinea pigs up to 310 days of age; the posterior (pos) curvature (dashed line, 2nd equation) was calculated as 10.23% less than the anterior radius (see text). (b) The radius of the anterior (solid line, 1st equation) and posterior (dashed line, 2nd equation) crystalline lens from frozen sections determined over the emmetropization period.

of the vitreous chamber depth (20 vs. 10 μm/day, respectively) and the anterior chamber expanded axially by 6 μm/day. The proportion of the axial length of the eye occupied by the anterior chamber (10.9%) remained constant over time, but an increasing proportion was occupied by the lens (2 days: 45%, 1000 days, 53% of the axial length; ratio: lens thickness/axial length $= 0.3461 + 0.0622 \times \log_{10}(40.5904 + \text{age})$) and a decreasing proportion by the vitreous chamber (2 days: 40%, 1000 days: 32%; ratio: lens thickness/axial length $= 0.4792 - 0.0536 \times \log_{10}(34.2779 + \text{age})$). This suggests that the axial changes in the eye may not be a consequence of simple scaling.

At 2 days of age, the thicknesses of the retina, choroid and sclera were approximately equal at 121, 120 and 126 μm, respectively. At 30 days of age, the retinal, choroidal and scleral thicknesses were 110, 139 and 125 μm. The choroid and sclera thickened with age, each by 43 μm over 1000 days, while that of the retina thinned by 26 μm over the same period (Fig. 3). This retinal thinning is approximately equivalent (within 9 μm) to the passive consequence of distributing the same retinal area around a larger eye, based on a hemispherical model in which the radius is the depth of the vitreous chamber. Overall, the total thickness of these posterior layers of the eye thickened continually with age (Fig. 3d) and were on average 352 μm at 30 days of age.

The inner 40% of the corneal surface, encompassing much of the pupil, was approximately spherical. The radius of curvature of the anterior corneal surface determined from infrared videokeratometry in awake guinea pigs increased with age (Fig. 4a) changing from 3.1 mm at 2 days to 4.4 mm at 300 days of age, the average rate of flattening being 4.3 μm/day. Estimates of corneal radius were 4.9% greater in the frozen sections, but were well correlated with those from the videokeratometry ($r^2 = 0.95$). The posterior corneal radius determined from frozen sections was on average 10.23% less than the frozen anterior radius, independent of age. The effect of reducing the anterior cor-

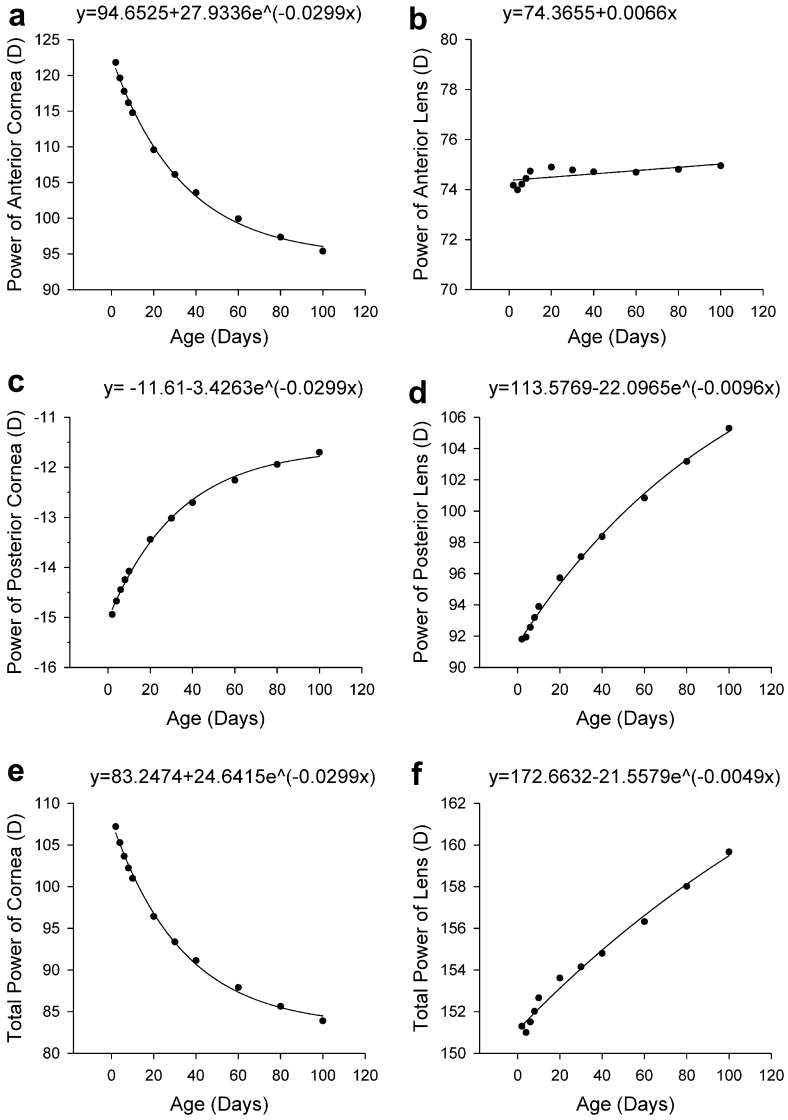

Fig. 5. Changes with age in the power of the cornea and lens from the schematic eye model. The equations for each fit are shown above each plot.

neal radius, as determined by videokeratometry, by this factor is shown by the dashed line in Fig. 4a, and the associated log fits were used in the schematic eye model.

The anterior surface of the crystalline lens was significantly flatter than the posterior surface (Fig. 4b, $p < .001$) and their respective radii also increased significantly with age ($p < .001$ in both cases), although more so for the anterior surface (16 μm/day) than for the posterior surface (9 μm/day).

3.3. Schematic eye model

Schematic eyes were developed from 2 to 100 days of age using the equations from Figs. 2 and 4. These models were constructed using the adjusted refractive error shown by the dashed line in Fig. 1c. The resulting power of the optical surfaces and their combinations are shown in Fig. 5 and the principal points, nodal points and focal points are plotted in Fig. 6, each showing how these parameters change as a function of age. The increase in the primary focal length ($f = 4.8418 - 0.4409 \times e^{-0.0343 \times age}$) and secondary focal length ($f' = 6.4619 - 0.5885 \times e^{-0.0343 \times age}$) slowed with age, but over the first 30 days was approximately linear ($r^2 = .98$ in both cases) and increased by 9.2 and 12.3 μm/day, respectively. An example schematic eye for a 10 day old guinea pig (refractive error of +0.9 D) is superimposed on a frozen section in Fig. 7a. (10 days was chosen as this age is useful to interpret the outcomes from experiments which manipulate refractive development.) All associated model parameters are shown in Fig. 7b. The detailed parameters for 30 and 100 day model eyes are shown in Table 1. The former represents the eye at the end of the emmetropization period, and the latter represents the eye well after sexual maturity which occurs at 75 days based on the mean time for females and males (Rowlands & Weir, 1984).

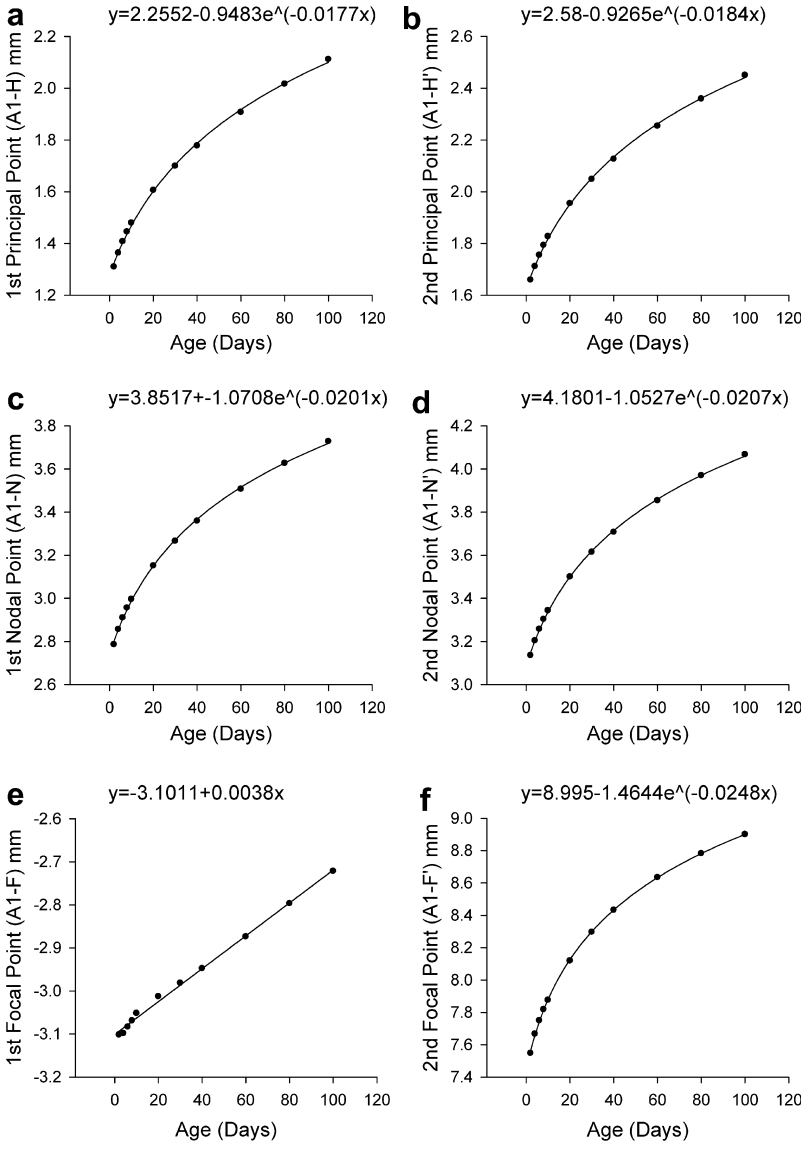

Fig. 6. Changes with age in the distance of the principal, focal and nodal points from the anterior corneal surface. The equations can be used to predict their location (y) for any age (x). e, exponential. Paraxial modelling used standard equations (see text) and was confirmed using OSLO Edu® software.

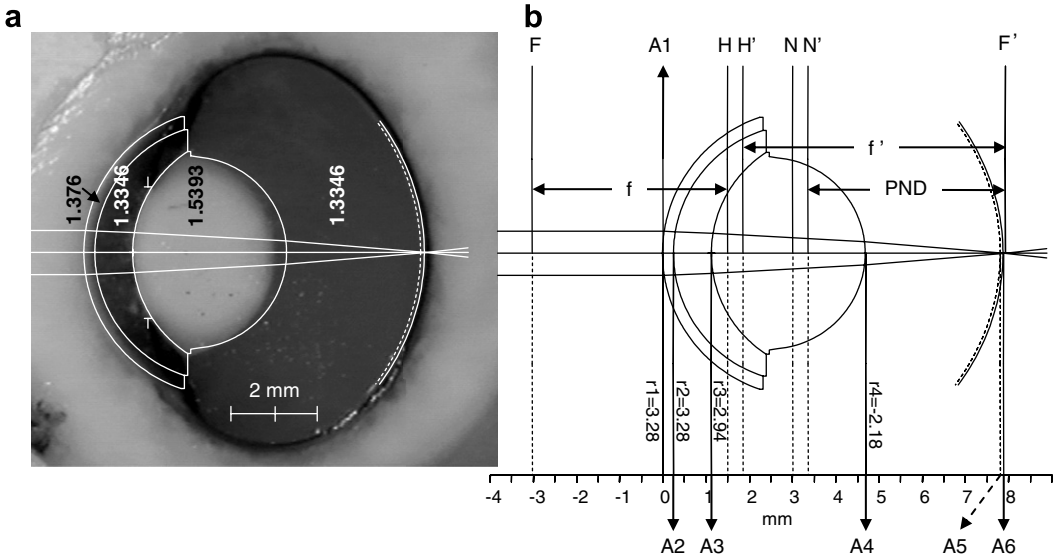

Fig. 7. Example schematic eye for a 10 day old guinea pig. (a) Frozen section of the eye with schematic eye from OSLO Edu® superimposed. The crystalline lens shifts slightly anteriorly in frozen sections. Four refractive indices are shown. (b) Detailed parameters of the schematic eye. $r1$–$r4$, radii; f, f', primary and secondary focal lengths; PND, posterior nodal distance; F, F', 1st and 2nd focal points; H, H', 1st and 2nd principal points; N, N', 1st and 2nd nodal points; position of surfaces are indicated as $A1$–$A6$. Dashed line at back of the eye is the retinal/vitreal interface, solid line is the retinal/choroidal interface.

The power of the guinea pig eye was 227 D at 2 days of age which decreased by 19.7 D by 100 days (Fig. 8a). At the end of the emmetropization period at 30 days of age, the power of the eye was 214 D. This declining power was due to a 22% decrease in corneal power between 2 and 100 days (reduced by 22 D, Fig. 5e) principally arising from a change in the power of the anterior surface (decrease of 26 D vs. increase of 3 D for anterior and posterior cornea, respectively, Fig. 5a,c). This decline in corneal power was partially offset by a small but consistent increase in the power of the lens totalling 8.4 D over 100 days (Fig. 5f) due to changes in the power of the posterior lens surface only (increased by 14 D, Fig. 5d). The significant flattening of the anterior lens surface during growth (Fig. 4b) did not change its anterior power because it was balanced by a rising equivalent homonogeneous refractive index of the lens, which had to increase linearly with age (Fig. 8b) to produce the refractive errors we used in our model. The equivalent refractive index of the lens increased from 1.528 at 2 days to 1.564 at 30 days ($p < .001$). Not surprisingly, these values were higher than that measured in our squashed lens preparations (2–30 days: 1.426–1.431, $p = .16$, $n = 16$). As expected, the mean refractive index of the lens core (1.529) was higher than of the cortex (1.402) in 3 eyes which were from animals aged 30 days. The refractive index of the vitreous humor did not vary significantly with age and the mean ($1.3346 \pm 7.79\text{E-}05$, $n = 21$) was used in all models.

3.4. Predictions from the schematic eye

The posterior nodal distance increased until approximately 100 days of age (Fig. 8c), but the rate of change declined with age, with the maximum rate occurring during the first week of life (13.2, 10.6, 8.3 and 6.5 μm/day; weeks 1–4, respectively). Thus, any emmetropization mechanism would need to be most active during early life, but it is also worth noting that emmetropia would need to be maintained until at least 100 days of age. Image magnification at the retina (PNDπ/180 mm/degree) increased with age and was approximately 80 μm/degree (Fig. 8c, dashed line) increasing by approximately 4.8 μm/degree over the first 30 days. During this 30 day emmetropization period, the ratio of PND to axial length declined at a faster rate than in older eyes (Fig. 8d; age 1–30, slope = −0.0012; age 70–100, slope = −0.0003) suggesting ocular growth does not entirely arise from simple scaling over this period. Nevertheless, the PND was highly correlated with axial length over 100 days ($\text{AxL} = 3.6239 \times \text{PND} - 8.6824$; $r^2 = 0.99$). The square of the f number (PND/entrance pupil diameter)^2 based on our entrance pupil diameters measured in infrared light (Fig. 1a), was very low and decreased from 1.3 to 0.7 between 2 and 100 days of age (f number$^2 = 0.5508 + 0.7648 \times e^{-0.0168 \times \text{age}}$) making the maximum potential brightness of the retinal image very high.

4. Discussion

4.1. Stages of ocular development

The axial growth of the eye and the rate of emmetropization in the guinea pig is similar to other species if aligned at the point of sexual maturity and scaled by the time taken to reach adulthood (Fig. 9). For this purpose, we considered the guinea pig to be an "infant" until weaned (at 3 weeks of age), a "juvenile" until the onset of sexual matu-

Table 1
Model eye parameters for the guinea pig eye at the end of the initial emmetropization period (30 days) and at 100 days of age (sexual maturity occurs at 75 days): refer to Fig. 7 for nomenclature

		Age (days)	
		30	100
Refractive indices			
$n2$	Cornea	1.376	1.376
$n3$	Aqueous	1.335	1.335
$n4$	Lens (homogeneous)	1.564	1.649
$n5$	Vitreous	1.335	1.335
$n6$	Retina	1.351	1.351
Distances (mm)			
$A1$–$A2$	Thickness of cornea	0.253	0.253
$A2$–$A3$	Anterior chamber depth	0.935	1.013
$A3$–$A4$	Thickness of lens	3.814	4.299
$A4$–$A5$	Vitreous chamber depth	3.114	3.205
$A5$–$A6$	Retinal thickness	0.110	0.105
$A6$–$A7$	Choroid thickness	0.139	0.147
$A7$–$A8$	Scleral thickness	0.125	0.134
$A1$–$A5$	Axial length	8.226	8.875
$A1$–$A8$	Ocular length	8.524	9.184
Radii (mm)			
$r1$	Anterior cornea	3.543	3.942
$r2$	Posterior cornea	3.180	3.539
$r3$	Anterior lens	3.061	4.188
$r4$	Posterior lens	−2.358	−2.981
Powers (D)			
	Anterior cornea	106.134	95.385
	Posterior cornea	−13.018	−11.700
	Total cornea	93.370	83.891
	Anterior lens	74.779	74.952
	Posterior lens	97.074	105.300
	Total lens	154.147	159.670
	Power of eye	213.613	206.906
Cardinal points (mm)			
$A1$–H	1st principal point	1.700	2.112
$A1$–H'	2nd principal point	2.049	2.451
$A1$–F	1st focal point	−2.981	−2.721
$A1$–F'	2nd focal point	8.297	8.901
$A1$–N	1st nodal point	3.266	3.729
$A1$–N'	2nd nodal point	3.615	4.068
Focal lengths (mm)			
N'–F'	Posterior nodal distance (f)	4.681	4.833
H'–F'	f'	6.248	6.450
	Refractive error (raw)	0.721	0.700
	Refractive error (adjusted)	0.021	0.000

rity (at 75 days based on the mean time for females and males, Rowlands & Weir, 1984), and an "adolescent" until it reached its adult body weight at around one year of age (Fig. 1a).

In many species, the axial length of the eye is typified by a rapid increase early in life which subsequently slows and becomes asymptotic as age increases (Fig. 9b). In humans, axial length increases by 25% over the first 2–3 years of life but only by 1% over the next ten or more years (Gordon & Donzis, 1985; Larsen, 1971b; Sorsby & Leary, 1969) and even less during adolescence (Fledelius, 1982; Zadnik, 1997). In the guinea pig, axial length also increases more during infancy (12% first 3 weeks, 8% during juvenile stage, 2% during the adolescent stage). Similar growth phases, albeit over different time scales, have been shown in the chick (Irving, Sivak, Curry, & Callender, 1996), tree shrew (Norton & McBrien, 1992), marmoset (Graham & Judge, 1999; Troilo & Judge, 1993) and macaque (Bradley et al., 1999). Graham and Judge (1999) propose ocular elongation in many species is approximately logarithmic with time, a view that concords with the data reported here for the guinea pig.

Age related increases in the depth of the anterior chamber occurs in many species (tree shrew: Norton & McBrien, 1992; marmoset: Graham & Judge, 1999; Troilo & Judge, 1993; macaque: Kiely et al., 1987; human: Larsen, 1971a; Pennie, Wood, Olsen, White, & Charman, 2001), and in the guinea pig the changes were well fitted by a logarithmic function. The developmental changes in the depth of the vitreous chamber are also generally logarithmic with time in infant and juvenile eyes of the marmoset, macaque, and human (Graham & Judge, 1999) and we found that the same was true for the guinea pig eye. In contrast, the vitreous chamber of the tree shrew eye, after initially increasing in size, decreases in depth (Norton, 1990).

The growth of the crystalline lens is more complex. Vertebrate lenses normally grow throughout life by the addition of fibre cells at the lens surface (Kuszak, Mazurkiewicz, & Zoltoski, 2006). While the lens of the tree shrew eye continually thickens with age (Norton & McBrien, 1992), the human lens has multiple stages of growth and has been reported to either show no change in thickness from childhood to 20 years (Manzitti, Darnel, Gamio, & Bennozi, 1994) or to thin between 6 and 10 years (Mutti et al., 1998; Zadnik, Mutti, Fusaro, & Adams, 1995) before steadily increasing during adult life (Cook, Koretz, Pfahnl, Hyun, & Kaufman, 1994). Similarly, age related changes in lens thickness in the marmoset eye are not monotonic. The maximum lens thickness in the marmoset is reached around ten weeks of age after which lens thickness declines (Graham & Judge, 1999). We find that the guinea pig lens increased in thickness, at least up to 825 days of age, but the rate of change was variable. Lens thickening could not be described a simple log function, and the rate of lens thickening became more rapid after emmetropization.

This variable change in the rate of thickening could be offset by concurrent changes in the refractive index of the lens to allow the maintenance of emmetropia. In our schematic eyes, we did find that the equivalent homonogeneous refractive index of the lens increased with age, however it is yet to be determined how this might translate within a multiple lens shell model.

4.2. The location of the retinoscopic reflex

If the retinoscopic reflex arose from the vitreal/retinal boundary (Glickstein & Millodot, 1970), the associated

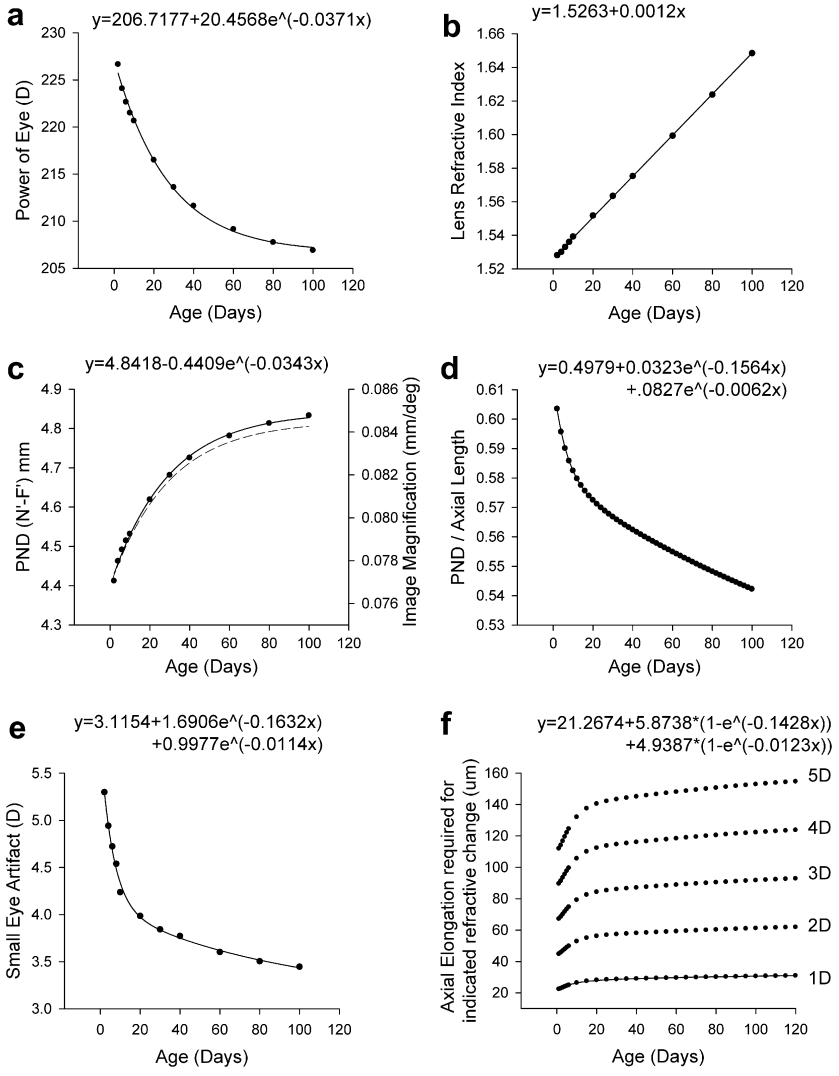

Fig. 8. Predictions from the schematic eye model. (a) The decline in the total power of the eye settles at approximately 100 days of age. (b) The homogeneous refractive index of the crystalline lens needed in the schematic eye to match the refractive error when adjusted to emmetropize to zero (dashed line in Fig. 1c). (c) The posterior nodal distance of the eye (filled circles and solid line, equation above, left axis) and retinal image magnification (dashed line, right axis) increases until approximately 100 days of age to a maximum of 0.084 mm/degree. (d) The ratio of the posterior nodal distance (PND) to the axial length declines with age. (e) The calculated hypothetical small eye artefact if it were the case that the retinoscopic reflex originated from the vitreal/retinal boundary. These refractive offsets are not supported by our model, which suggests that there is no artefact in the guinea pig eye and the white light reflex originates from the photoreceptor plane (see text). (f) Calculated increases in axial length required to create 1–5 D of myopia in the schematic eyes at different ages. The equation of the fit for 1 D of myopia is shown above.

small eye artefact (Fig. 8e) should have been +5.5 D in newborn guinea pigs, +3.8 D in a 30 day old animal and stablising to +3.1 D in adults. Instead, we found a stable refractive error of only +0.7 D after 30 days of age when using white light retinoscopy. It seems unlikely that the guinea pig is born myopic and "emmetropizes" to an even greater myopic refractive error, and more plausible that +0.7 D represents the real hyperopic artefact. The schematic eye model predicts that an artefact of +0.7 D means the reflex originated, not from the vitreal/retinal boundary, but approximately 20 μm in front of the retinal/choridal boundary (Fig. 8f). This coincides approximately with the plane of the outer segments of the photoreceptors. Thus, we conclude that there is no small eye artefact in the adult pigmented guinea pig eye.

4.3. Ocular size, image brightness and lifestyle

The axial length of the guinea pig eye increases with increasing body weight (2 days: 7.3 mm, 105 gm; 30 days: 8.3 mm, 327 gm; adult at 1 year, 9.6 mm, 946 gm; body weight = 1.3 × axial length + 7.86, $p < .001$). The slope of the relationship between body weight (kgs) and axial length (mm) between 30 and 100 days of age is 1.3, being more than would be expected from allometric considerations alone, but similar to other small mammalian eyes. This suggests the size of the body constrains the size of the eye and imposes a common space constraint between different species (Hughes, 1977b) and in individual species as they age. Improved resolution in the image plane over and above isomorphic scaling could occur if the *f*-number is

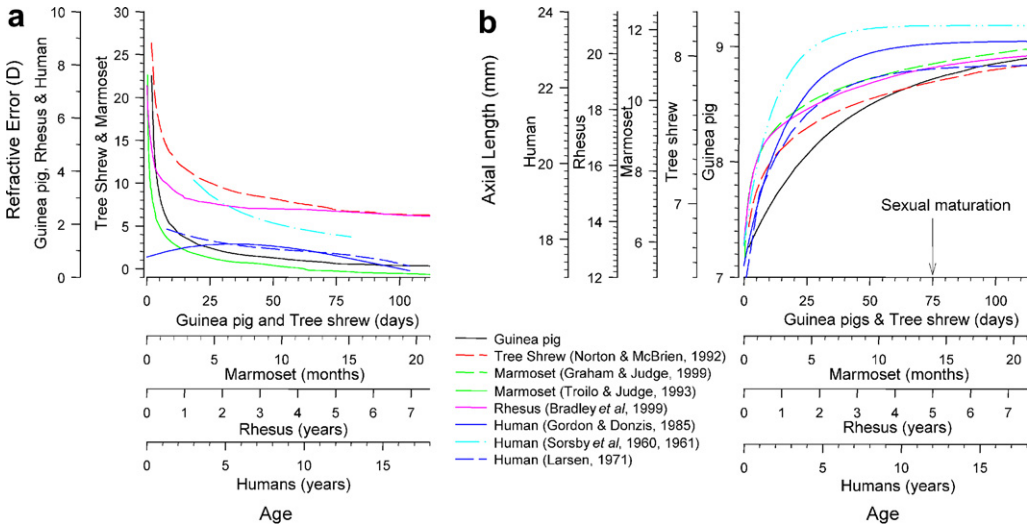

Fig. 9. Comparision of emmetropization in different species. (a) Refractive error; (b) Axial length. The relevant scale is located to the right (y-axis) or above (x-axis) the species name. The x-axis scales are aligned based on the time of sexual maturity. The y-axis scale is arbitrarily aligned for clarity.

increased and if the sampling grain is reduced. It is likely that photoreceptor spacing is already minimised in small mammalian eyes (Barlow, 1981). This is likely to be true in the guinea pig eye, as the photoreceptors are predominately rods (92% to 83% depending on retinal location, Peichl & Gonzalez-Soriano, 1994) which average 2 μm in diameter (Matthews, 1991). However, we find that the f-number is relatively low in the guinea pig, suggesting that resolution is perhaps not the primary design consideration. However, lower f-numbers allow a higher maximum retinal image brightness and occur in noctural species when compared with diurnal animals of similar eye size (Hughes, 1977b; Martin, 1994).

Guinea pigs are active during both the day and night, sleep for multiple short periods during both periods with 6.8% more sleep time during the light period (Tobler, Franken, & Jaggi, 1993) and have no clear circadian heart rate rhythmicity (Akita, Ishii, Kuwahara, & Tsubone, 2001). There is confusion as to whether the guinea pig is adapted for nocturnal or diurnal conditions. However, the presence of night activity and tendency to burrow and preference for hiding suggests that they may be at least partially adapted for nocturnal or crepuscular conditions. The schematic eye also suggests that the guinea pig eye is potentially adapted for nocturnal conditions. The (f-number)^2 of the guinea pig eye changes with age and ranges between 1.3 (2 day) and 0.55 (adult) for an axial lengths of 7.3 and 9.6 mm, respectively. These values lie on the relationship line that is defined by other species with regular nocturnal activity (Martin, 1994; Hughes, 1977b). In contrast, the diurnal starling eye, although of a similar eye size, has a (f-number)^2 which is 6 times greater (Martin, 1994). For a given axial length, the light gathering power of the eye is greater in nocturnal species, and has been estimated by Hughes (1977b cf. his Fig. 10) to be approximated by the square of the maximum pupil diameter plotted against the square of the power of the eye. In the guinea pig eye, pupil diameter^2 to power^2 ranges from 15:51,270 (2 days old); 22:45,556 (30 days) to 43:42,732 at 1 year of age. Thus the guinea pig eye lies close to that of other nocturnal species and is similar to the badger (Hughes, 1977b).

Optical design for noctural versus diurnal habitats also involves the ratio of lens to corneal power. A smaller brighter image of a scaled nocturnal eye is achieved when the ratio of lens power to total power of the eye is relatively high. In the guinea pig it is between 72% (30 days) and 83% (1 year). The more posterior position of the lens in nocturnal species increases image brightness, but to maintain emmetropia the increased anterior chamber depth requires a greater lens power compared to that in a similarly sized eye of a diurnal species. In the guinea pig, the ratio of lens power to corneal power (30 day: 1.7, adult: 2.0) is similar to other species with regular noctural activity when scaled for axial length (Martin, 1994). Taken together, these data suggest that the guinea pig eye is primarily designed to maximise image brightness in dim light conditions. This is despite the presence of mid-, and short-, wavelength sensitive cones (Parry & Bowmaker, 2002; Rohlich, van Veen, & Szel, 1994) and behaviorally demonstrated dichromatic visual capacity (Jacobs & Deegan, 1994).

4.4. Use of the guinea pig in models of refractive development

The growth of the guinea pig eye can be easily manipulated in models of refractive development (Howlett & McFadden, 2006; Lu et al., 2006; McFadden et al., 2004). The schematic eye predicts that an axial myopia of 1 D occurs when there is an ocular elongation of 23 μm (2 days) to 32 μm (1 year) (Fig. 8f). The guinea pig eye has also been found to compensate for defocus imposed through spectacle lenses (Howlett, 2003; McFadden et al., 2004; Wallman & McFadden, 1995). In experiments which

aim to influence refractive development and induce spectacle lens compensation, the maximum refractive change is approximately ±4 D, equivalent to a maximum axial change of ±127 μm (Fig. 8f). However, compensation over short periods is not necessarily complete and environmental factors can cause a combination of both optical and axial myopia (Howlett & McFadden, 2006), and thus the elongation changes are somewhat smaller in practise. As a minimum, a resolution of approximately 2 D is desirable. Thus, when using the guinea pig for a model of refractive development, it is necessary to use imaging techniques for measuring ocular elongation which can discriminate changes of the order of approximately 50 μm.

We have shown that emmetropization in the guinea pig eye occurs within 1 month after birth with the largest changes in the rate of growth occurring just after birth. Therefore, when manipulating visual input to the guinea pig eye in experiments which aim to influence refractive development, greater effects might be expected to be found in younger eyes. Further, the declining PND to axial length ratio in the schematic model eye suggests that the components of the eye do not grow in a simple proportional manner, even after emmetropia is reached. Thus, some active mechanism must exist which underlies emmetropization as well as the maintenance of emmetropia.

Acknowledgments

We are grateful for the help of Dr. John Holdsworth, Dept. of Physics, University of Newcastle for help in preliminary ray tracing analysis, to Natalia Avila, School of Psychology, The University of Newcastle for assistance with using OSLO, and to Eleanor Huber, School of Psychology, The University of Newcastle for animal care and husbandry.

References

Akita, M., Ishii, K., Kuwahara, M., & Tsubone, H. (2001). The daily pattern of heart rate, body temperature, and locomotor activity in guinea pigs. *Experimental Animals, 50*, 409–415.

Andison, M. E., Sivak, J. G., & Bird, D. M. (1992). The refractive development of the eye of the American kestrel (*Falco sparverius*): a new avian model. *Journal of Comparative Physiology [A], 170*, 565–574.

Barlow, H. B. (1981). The ferrier lecture, 1980. Critical limiting factors in the design of the eye and visual cortex. *Proceedings of the Royal Society of London, Series B, Biological Sciences, 212*, 1–34.

Bradley, D. V., Fernandes, A., Lynn, M., Tigges, M., & Boothe, R. G. (1999). Emmetropization in the rhesus monkey (*Macaca mulatta*): birth to young adulthood. *Investigative Ophthalmology and Visual Science, 40*, 214–229.

Castro, M. R., Lutz, D., & Edelman, J. L. (2004). Effect of COX inhibitors on VEGF-induced retinal vascular leakage and experimental corneal and choroidal neovascularization. *Experimental Eye Research, 79*, 275–285.

Cook, R. C., & Glasscock, R. E. (1951). Refractive and ocular findings in the newborn. *American Journal of Ophthalmology, 34*, 1407–1413.

Cook, C. A., Koretz, J. F., Pfahnl, A., Hyun, J., & Kaufman, P. L. (1994). Aging of the human crystalline lens and anterior segment. *Vision Research, 34*, 2945–2954.

Ehrlich, D. L., Atkinson, J., Braddick, O., Bobier, W., & Durden, K. (1995). Reduction of infant myopia: a longitudinal cycloplegic study. *Vision Research, 35*, 1313–1324.

Fledelius, H. C. (1982). Ophthalmic changes from age of 10 to 18 years. A longitudinal study of sequels to low birth weight. IV. Ultrasound oculometry of vitreous and axial length. *Acta Ophthalmologica (Copenh), 60*, 403–411.

Foster, C. S., Zelt, R. P., Mai-Phan, T., & Kenyon, K. R. (1982). Immunosuppression and selective inflammatory cell depletion. Studies on a guinea pig model of corneal ulceration after ocular alkali burning. *Archives of Ophthalmology, 100*, 1820–1824.

Glickstein, M., & Millodot, M. (1970). Retinoscopy and eye size. *Science, 168*, 605–606.

Gordon, R. A., & Donzis, P. B. (1985). Refractive development of the human eye. *Archives of Ophthalmology, 103*, 785–789.

Graham, B., & Judge, S. J. (1999). Normal development of refractive state and ocular component dimensions in the marmoset (*Callithrix jacchus*). *Vision Research, 39*, 177–187.

Gwiazda, J., Thorn, F., Bauer, J., & Held, R. (1993). Emmetropization and the progression of manifest refraction in children followed from infancy to puberty. *Clinical Vision Science, 8*, 337–344.

Helmholtz, H. v. (1925). Treatise on physiological optics. In J. P. Southall (Ed.) (New York: Dover Publications (Original work)).

Howlett, M.H.C. (2003). The visual regulation of eye growth and refractive error in the guinea pig. PhD Thesis (pp. 1–254). Newcastle: University of Newcastle, Australia.

Howlett, M. H., & McFadden, S. A. (2006). Form-deprivation myopia in the guinea pig (*Cavia porcellus*). *Vision Research, 46*, 267–283.

Hughes, A. (1972). A schematic eye for the rabbit. *Vision Research, 12*, 123–138.

Hughes, A. (1977a). The refractive state of the rat eye. *Vision Research, 17*, 927–939.

Hughes, A. (1977b). The topography of vision in mammals of contrasting life styles: comparative optics and retinal organisation. In F. Crescitelli (Ed.). *The visual system in vertebrates* (VII/5, pp. 615–756). Berlin: Springer-Verlag.

Hughes, A. (1979). A schematic eye for the rat. *Vision Research, 19*, 569–588.

Irving, E. L., Sivak, J. G., Curry, T. A., & Callender, M. G. (1996). Chick eye optics: zero to fourteen days. *Journal of Comparative Physiology. A, Sensory, Neural, and Behavioral Physiology, 179*, 185–194.

Jacobs, G. H., & Deegan, J. F. 2nd, (1994). Spectral sensitivity, photopigments, and color vision in the guinea pig (*Cavia porcellus*). *Behavioral Neuroscience, 108*, 993–1004.

Kiely, P. M., Crewther, S. G., Nathan, J., Brennan, N. A., Efron, N., & Madigan, M. A. (1987). A comparison of ocular development development of the cynomolgus monkey and man. *Clinical Vision Science*, 269–280.

Kuszak, J. R., Mazurkiewicz, M., & Zoltoski, R. (2006). Computer modeling of secondary fiber development and growth: I. *Nonprimate lenses. Molecular vision [electronic resource], 12*, 251–270.

Larsen, J. S. (1971a). The sagittal growth of the eye. II. Ultrasonic measurement of the axial diameter of the lens and the anterior segment from birth to puberty. *Acta Ophthalmologica, 49*, 427–440.

Larsen, J. S. (1971b). The sagittal growth of the eye. IV. Ultrasonic measurement of the axial length of the eye from birth to puberty. *Acta Ophthalmologica, 49*, 873–886.

Loeliger, M., & Rees, S. (2005). Immunocytochemical development of the guinea pig retina. *Experimental Eye Research, 80*, 9–21.

Lu, F., Zhou, X., Zhao, H., Wang, R., Jia, D., Jiang, L., et al. (2006). Axial myopia induced by a monocularly-deprived facemask in guinea pigs: a non-invasive and effective model. *Experimental Eye Research, 82*, 628–636.

Manzitti, E., Darnel, A., Gamio, S., & Bennozi, J. (1994). Eye length in congenital cataracts. In E. Cotlier, S. Lambert, & D. Taylor (Eds.), *Congenital cataracts* (pp. 251–259). RG Landes.

Martin, G. R. (1994). Form and function in the optical structure of bird eyes. In M. N. O. Davies & P. R. Green (Eds.), *Perception and motor control in birds* (pp. 5–34). Springer-Verlag.

Matthews, H. R. (1991). Incorporation of chelator into guinea-pig rods shows that calcium mediates mammalian photoreceptor light adaptation. *Journal of Physiology, 436*, 93–105.

Mayer, D. L., Hansen, R. M., Moore, B. D., Kim, S., & Fulton, A. B. (2001). Cycloplegic refractions in healthy children aged 1 through 48 months. *Archives of Ophthalmology, 119*, 1625–1628.

McFadden, S. A., Howlett, M. H., & Mertz, J. (2004). Retinoic acid signals the direction of ocular elongation in the guinea pig eye. *Vision Research, 44*, 643–653.

Mutti, D. O., Zadnik, K., Fusaro, R. E., Friedman, N. E., Sholtz, R. I., & Adams, A. J. (1998). Optical and structural development of the crystalline lens in childhood. *Investigative Ophthalmology and Visual Science, 39*, 120–133.

Mutti, D. O., Zadnik, K., Johnson, C. A., Howland, H. C., & Murphy, C. J. (1992). Retinoscopic measurement of the refractive state of the rat. *Vision Research, 32*, 583–586.

Norton, T. T. (1990). Experimental myopia in tree shrews. In G. R. Bock & K. Widdows (Eds.). *Myopia and the control of eye growth* (Vol. 155, pp. 178–194). West Sussex: John Wiley & Sons.

Norton, T. T., & McBrien, N. A. (1992). Normal development of refractive state and ocular component dimensions in the tree shrew (*Tupaia belangeri*). *Vision Research, 32*, 833–842.

Ofri, R., Millodot, S., Shimoni, R., Horowitz, I. H., Ashash, E., & Millodot, M. (2001). Development of the refractive state in eyes of ostrich chicks (*Struthio camelus*). *American Journal of Veterinary Research, 62*, 812–815.

Parry, J. W., & Bowmaker, J. K. (2002). Visual pigment coexpression in Guinea pig cones: a microspectrophotometric study. *Investigative Ophthalmology and Visual Science, 43*, 1662–1665.

Peichl, L., & Gonzalez-Soriano, J. (1994). Morphological types of horizontal cell in rodent retinae: a comparison of rat, mouse, gerbil, and guinea pig. *Visual Neuroscience, 11*, 501–517.

Pennie, F. C., Wood, I. C., Olsen, C., White, S., & Charman, W. N. (2001). A longitudinal study of the biometric and refractive changes in full-term infants during the first year of life. *Vision Research, 41*, 2799–2810.

Rohlich, P., van Veen, T., & Szel, A. (1994). Two different visual pigments in one retinal cone cell. *Neuron, 13*, 1159–1166.

Rowlands, I. W., & Weir, B. J. (1984). Mammals: non-primate eutherians. In G. E. Lamming (Ed.). *Reproductive cycles of vertebrates* (Vol. 1, pp. 455–658). Edinburgh, Melbourne, New York: Churchill Livingston.

Saunders, K. J., Woodhouse, J. M., & Westall, C. A. (1995). Emmetropisation in human infancy: rate of change is related to initial refractive error. *Vision Research, 35*, 1325–1328.

Schaeffel, F., Glasser, A., & Howland, H. C. (1988). Accommodation, refractive error and eye growth in chickens. *Vision Research, 28*, 639–657.

Schmucker, C., & Schaeffel, F. (2004). A paraxial schematic eye model for the growing C57BL/6 mouse. *Vision Research, 44*, 1857–1867.

Simpanya, M. F., Ansari, R. R., Suh, K. I., Leverenz, V. R., & Giblin, F. J. (2005). Aggregation of lens crystallins in an in vivo hyperbaric oxygen guinea pig model of nuclear cataract: dynamic light-scattering and HPLC analysis. *Investigative Ophthalmology and Visual Science, 46*, 4641–4651.

Sorsby, A., Benjamin, B., & Sheridan, M. (1961). Refraction and its components during the growth of the eye from the age of three. *Special Report Series Medical Research Council* (Vol. 301, pp. 1–67). London: H.M. Stationary Office.

Sorsby, A., & Leary, G. A. (1969). A longitudinal study of refraction and its components during growth. *Special Report Series Medical Research Council* (Vol. 309, pp. 1–41). London: H.M. Stationary Office.

Sorsby, A., & Sheridan, M. (1960). The eye at birth: measurement of the principal diameters in 48 cadavers. *Journal of Anatomy (London), 94*, 193.

Spira, A. W. (1975). In utero development and maturation of the retina of a non-primate mammal: a light and electron microscopic study of the guinea pig. *Anatomy and Embryology, 146*, 279–300.

Tobler, I., Franken, P., & Jaggi, K. (1993). Vigilance states, EEG spectra, and cortical temperature in the guinea pig. *American Journal of Physiology, 264*, R1125–R1132.

Troilo, D., & Judge, S. J. (1993). Ocular development and visual deprivation myopia in the common marmoset (*Callithrix jacchus*). *Vision Research, 33*, 1311–1324.

Vakkur, G. J., & Bishop, P. O. (1963). The schematic eye in the cat. *Vision Research, 61*, 357–381.

Wallman, J., Adams, J. I., & Trachtman, J. N. (1981). The eyes of young chickens grow toward emmetropia. *Investigative Ophthalmology and Visual Science, 20*, 557–561.

Wallman, J., & McFadden, S. (1995). Monkey eyes grow into focus. *Nature (Medicine), 1*, 737–739.

Wallman, J., & Winawer, J. (2004). Homeostasis of eye growth and the question of myopia. *Neuron, 43*, 447–468.

Westheimer, G. (2006). Specifying and controlling the optical image on the human retina. *Progress in Retinal Eye Research, 25*, 19–42.

Wood, I. C., Hodi, S., & Morgan, L. (1995). Longitudinal change of refractive error in infants during the first year of life. *Eye, 9*, 551–557.

Zadnik, K. (1997). Myopia development in childhood. *Optometry and Vision Science, 74*, 603–608.

Zadnik, K., Mutti, D. O., Fusaro, R. E., & Adams, A. J. (1995). Longitudinal evidence of crystalline lens thinning in children. *Investigative Ophthalmology and Visual Science, 36*, 1581–1587.

Zhou, X., Qu, J., Xie, R., Wang, R., Jiang, L., Zhao, H., et al. (2006). Normal development of refractive state and ocular dimensions in guinea pigs. *Vision Research, 46*, 2815–2823.